Digest Journal of Nanomaterials and Biostructures Vol. 7, No. 3, July - September 2012, p. 1271 - 1277

RESOLUTION OF DIRECT PROBLEM BY THE FINITE ELEMENT METHOD: APPLICATION IN NEAR INFRA-RED OPTICAL MEDICAL IMAGING

SAOULI ABDELALI*, MANSOUR KARIM
Laboratory of Electronic Materials Study for Medical Applications (LEMEAMED), Campus Ahmed Hamani, Route Ain El Bey, Constantine, 25000 Algeria

The diffuse optical tomography (DOT) based on detection of a near InFra-Red Pulse (NIRP) called Time Pulse Spread Function (TPSF) and simulation of propagation of this pulse source. By combining measured and simulated TPSF can be reconstructed an optical image. Therefore, in this work we present the simulation of NIRP propagation in biological tissue and the influence of source frequency. This simulation is based on finite element method (FEM).

(Received June 18, 2012; Accepted September 1, 2012)

Keywords: Diffuse optical tomography, Time Pulse Spread Function, Finite element method.

1. Introduction

Diffuse optical tomography is a non invasive imaging technique that utilizes near-infrared light to probe highly scattering media [1]. In recent years, molecular imaging has emerged as an investigative tool for pre-clinical imaging of optical reporter probes in small animals [2]. Optical tomography imaging techniques can be classified based on the excitation mechanism employed: continuous-wave methods based on steady state excitation sources [3]-[4], frequency-domain methods which use frequency modulated (MHz) sources [5]-[6], and time-domain methods [7]-[8] based on short (~ fs-ps) laser pulses in conjunction with time resolved detection. Time domain measurements offer the most comprehensive information among the three techniques, since a single laser pulse implicitly contains all modulation frequencies, including the continuous-wave (zero frequency) component [9]. The quality of the reconstructed image depends strongly on the accuracy of the forward model [10]. In homogeneous mediums there exist analytical solutions for more complex geometries, such as circles, semi-infinite spheres or mediums which were developed and detailed in [11].

Thus, the method of finite elements is a digital method which is used to resolve the problems in the limits characterized by an equation with partial derivates and a set of conditions in the limits [12], which is the case of the forward model in optical tomography.

Indeed, a model of Finite Element Method (FEM) for solving the diffusion equation numerically offers advantages in speed and flexibility in comparison with other models [13]. Generally, the reconstruction of optical parameter does not use the complete form of TPSF calculated because it takes a lot of computing time, so there are some parameters calculated from TPSF to simplify this time such as mean time, mean value and variance of TPSF. Thus, the optical source has a significant role in reconstruction of the optical image [14]. In this work we use FEM in resolution of forward model and study the influence of frequency source on these parameters.

* Corresponding author: Abdou.zezou@yahoo.fr

2. Finite element approach

The propagation of light through a biological tissue is controlled by the radiative transfer equation (RTE) [15]. In the regions where tissue is highly scattering, RTE can be well approximated by a diffusion equation [16] (equation (1)):

$$-\nabla \frac{c}{3\left(\mu_a + \mu_s'\right)} \vec{\nabla} \varphi\left(\vec{r}, t\right) + \frac{\delta\varphi\left(\vec{r}, t\right)}{\delta t} + c\mu_a \varphi\left(\vec{r}, t\right) = S_0\left(\vec{r_0}, t\right) \quad (1)$$

Where:

c: The speed of light in vacuum. μ_a: Absorption Coefficient. μ_s': Reduces diffusion Coefficient. $S_0\left(\vec{r_0}, t\right)$: Local source of the photon. $\varphi\left(\vec{r}, t\right)$: Photons Intensity.

In two dimensions the equation (1) can be simplified to the following form:

$$\frac{\delta}{\delta x}\left(\alpha_x \frac{\delta}{\delta x}\varphi(x,y,t)\right) + \frac{\delta}{\delta y}\left(\alpha_y \frac{\delta}{\delta y}\varphi(x,y,t)\right) + \frac{\delta\varphi(x,y,t)}{\delta t} + \beta\varphi(x,y,t) = g \quad (2)$$

With:

$$\alpha_x = \alpha_y = -\frac{c}{3\left(\mu_a + \mu_s'\right)} \quad , \quad \beta = c\mu_a \quad , \quad g = cS_0\left(x_0, y_0, t\right)$$

For the heterogeneous geometries there is no analytical solution of the RTE, so we must use the numerical methods. One convenient numerical method in our field is FEM. We used the triangular shape of the elements since it is the most suitable for the irregular forms such as biological tissues.

Our system can conveniently be expressed in matrix form as in equation (2) [14]

$$\begin{bmatrix} M_{11}^e & M_{12}^e & M_{13}^e \\ M_{21}^e & M_{22}^e & M_{23}^e \\ M_{31}^e & M_{32}^e & M_{33}^e \end{bmatrix} \begin{Bmatrix} (\varphi_1^e)^n \\ (\varphi_2^e)^n \\ (\varphi_3^e)^n \end{Bmatrix} + \frac{1}{dt} \begin{bmatrix} MM_{11}^e & MM_{12}^e & MM_{13}^e \\ MM_{21}^e & MM_{22}^e & MM_{23}^e \\ MM_{31}^e & MM_{32}^e & MM_{33}^e \end{bmatrix} \begin{Bmatrix} (\varphi_1^e)^n \\ (\varphi_2^e)^n \\ (\varphi_3^e)^n \end{Bmatrix} +$$

$$\begin{bmatrix} T_{11}^e & T_{12}^e & T_{13}^e \\ T_{21}^e & T_{22}^e & T_{23}^e \\ T_{31}^e & T_{32}^e & T_{33}^e \end{bmatrix} \begin{Bmatrix} (\varphi_1^e)^n \\ (\varphi_2^e)^n \\ (\varphi_3^e)^n \end{Bmatrix} = \begin{Bmatrix} f_1^e \\ f_2^e \\ f_3^e \end{Bmatrix} + \begin{Bmatrix} p_1^e \\ p_2^e \\ p_3^e \end{Bmatrix} + \quad (3)$$

$$\frac{1}{dt} \begin{bmatrix} MM_{11}^e & MM_{12}^e & MM_{13}^e \\ MM_{21}^e & MM_{22}^e & MM_{23}^e \\ MM_{31}^e & MM_{32}^e & MM_{33}^e \end{bmatrix} \begin{Bmatrix} (\varphi_1^e)^{n-1} \\ (\varphi_2^e)^{n-1} \\ (\varphi_3^e)^{n-1} \end{Bmatrix}$$

Where:

$$M_{ij}^e = -\iint_{\Omega^e} \left[\alpha_x \left(\frac{\delta N_i}{\delta x}\right)\left(\frac{\delta Nj}{\delta x}\right) + \alpha_y \left(\frac{\delta N_i}{\delta y}\right)\left(\frac{\delta N_i}{\delta y}\right) \right] dxdy \quad (4)$$

$$MM_{ij}^e = \iint_{\Omega^e} N_i N_j dxdy \quad (5)$$

$$T_{ij}^e = \iint_{\Omega^e} \beta\, N_i N_j dxdy \quad (6)$$

$$f_i^e = \iint_{\Omega^e} N_i g\, dxdy \quad (7)$$

$$p_i^e = -\oint_{\Gamma^e} N_i \left(\alpha_x \frac{\delta}{\delta x}\varphi(x,y,t) n_x + \alpha_y \frac{\delta}{\delta y}\varphi(x,y,t) n_y \right) dl \quad (8)$$

In a more compact form, the matrix system from equation (3) can be expressed as:

$$\begin{bmatrix} K_{11}^e & K_{12}^e & K_{13}^e \\ K_{21}^e & K_{22}^e & K_{23}^e \\ K_{31}^e & K_{32}^e & K_{33}^e \end{bmatrix} \begin{Bmatrix} (\varphi_1^e)^n \\ (\varphi_2^e)^n \\ (\varphi_3^e)^n \end{Bmatrix} = \begin{Bmatrix} b_1^e \\ b_2^e \\ b_3^e \end{Bmatrix} \tag{9}$$

Where:

$$K_{ij}^e = M_{IJ}^e + MM_{IJ}^e + T_{IJ}^e$$

$$b_i^e = f_i^e + p_i^e + \sum_{j=1}^{3} MM_{ij}^e \left(\varphi_j^e\right)^{n-1} \tag{10}$$

This work is based on two dimension cut of cylinder form of phantom contain three inclusions with different optical properties ‘‘Figure. 1’’.

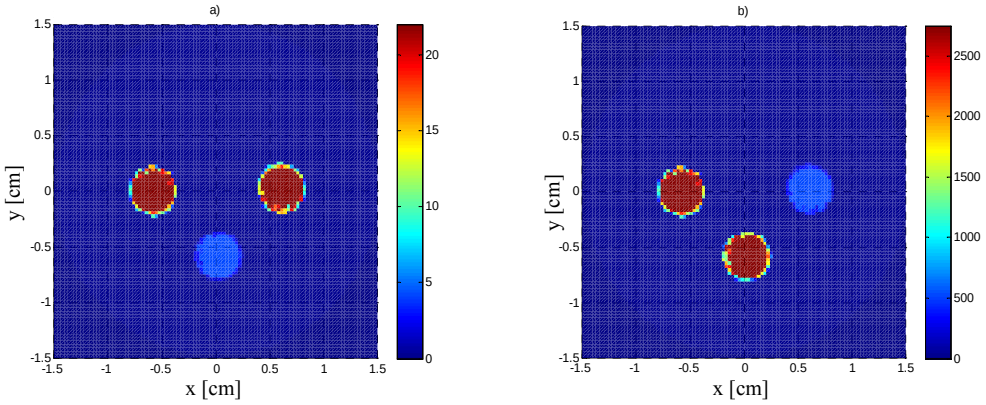

Fig. 1, a) Absorption Coefficient μ_a [m^{-1}].b) diffusion reduced Coefficient $\mu_s^{'}$ [m^{-1}].

We use Dirichlet and Robin boundary conditions presented in equation (11) (DBC) and equation (12) (RBC) respectively.

$$\varphi(\vec{r},t) = 0 \tag{11}$$

$$\varphi(\vec{r},t) + 2\frac{1}{3(\mu_a + \mu_s^{'})}\frac{1+R}{1-R}\frac{\partial\varphi(\vec{r},t)}{\partial n} = 0 \tag{12}$$

Where, n is a normal vector and $(R = 0)$ is the reflection parameter.

The simulation is based on three sources of a near infrared pulse with temporal and spectral profile presented in ‘‘Figure. 2’’.Each source is localised in Cartesian coordinates (x_0, y_0) = (0,-1.5*10^{-3}), see ‘‘Figure. 3. b’’. The spectral profile presents two peaks, see ‘‘Figure. 2. a2, b2, c2 ’’, where the peak on the right is mirror of the ones on the left. This mirror effect is due to the sampling of the impulse signals, which always create a mirror spectrum around the sampling frequency. Thus each source has its frequency and wavelength as follows, Source1: (f_1=1.48 [THz], λ_1=202.70 [µm]), Source2: (f_2=0.5 [THz], λ_2=600 [µm]), Source3: (f_3=50 [GHz], λ_3=6 [mm]), but all sources have the same intensity.

The mesh of our phantom is presented in ‘‘Figure. 3’’, where the areas which the optical properties are different to the principal phantom and with the close relations at the borders are finer mesh.

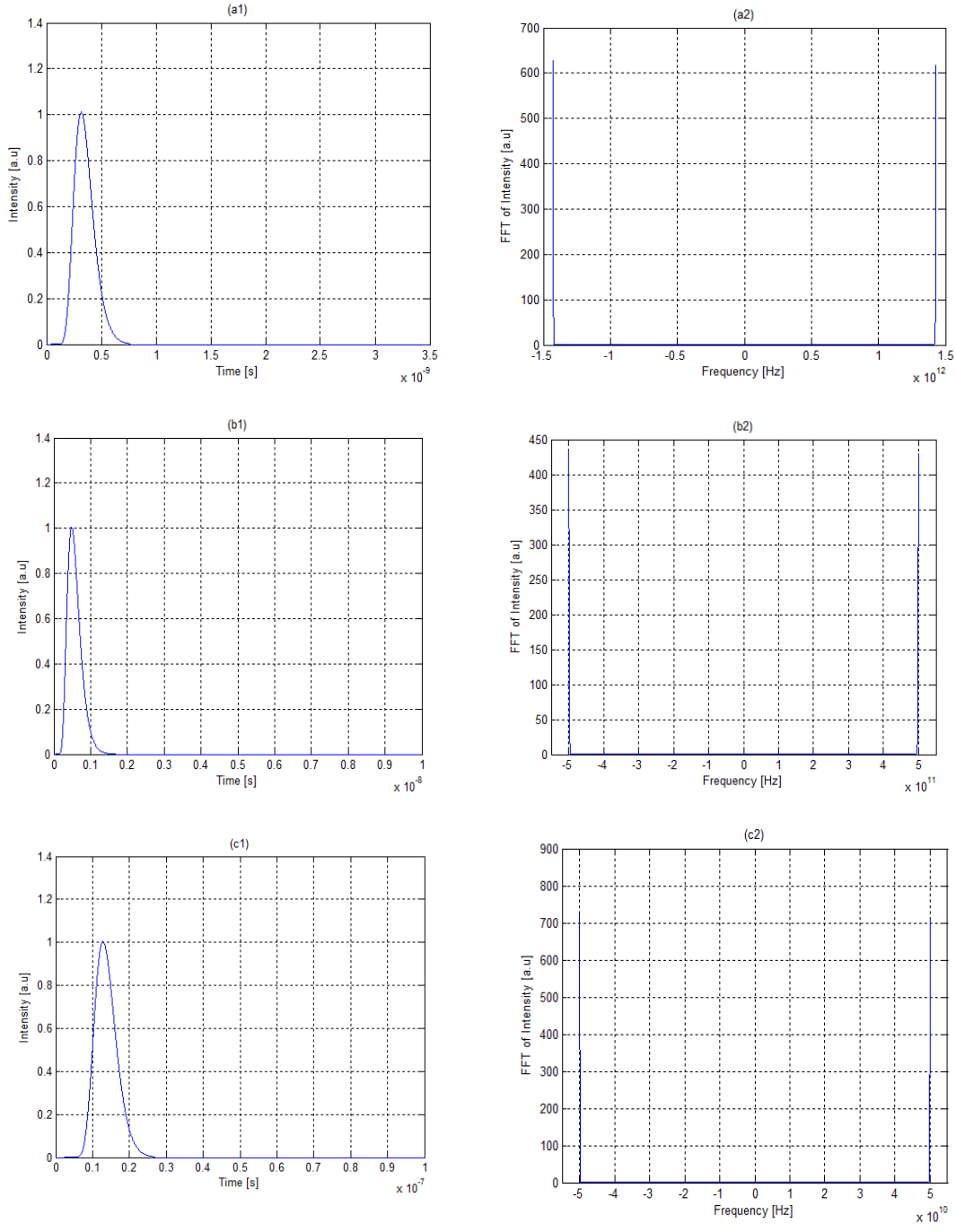

Fig2, a) Object tests mesh in 2D (1526 nodes, 2814 elements). b) Source and Detectors position.

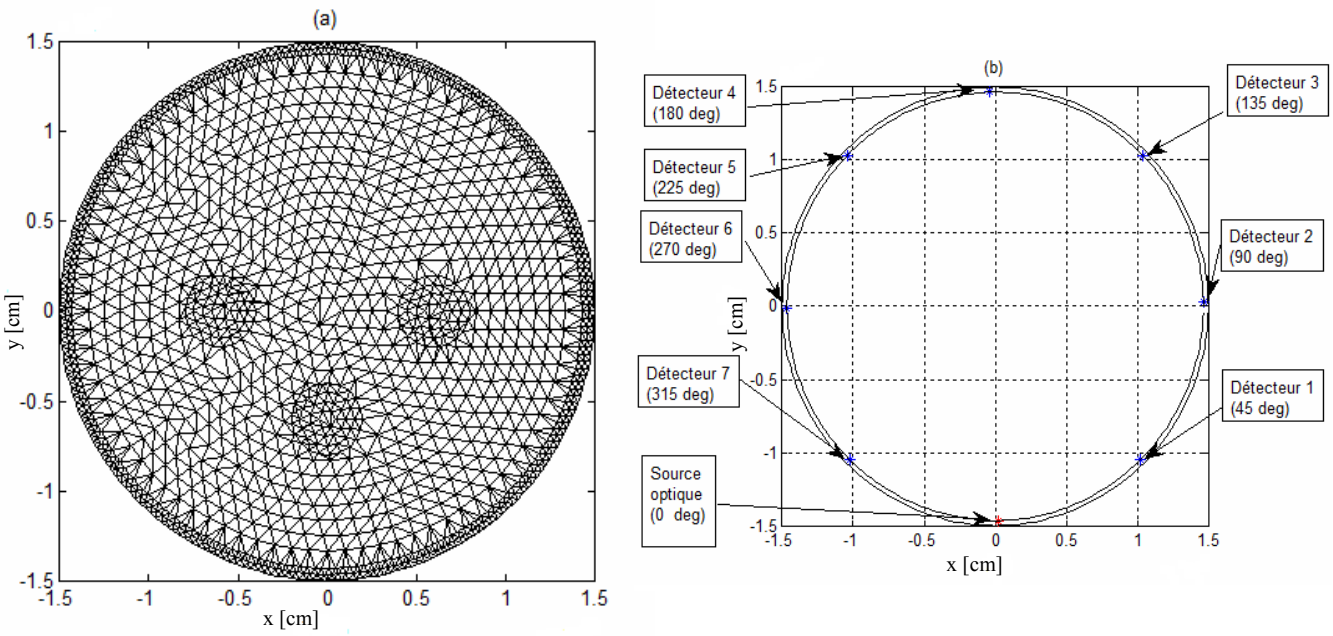

Fig3, a) Object tests mesh in 2D (1526 nodes, 2814 elements). b) Source and Detectors position.

3. Results and discussion

In this section we study the influence of the sources on a range of parameters, by comparing the results obtained for different frequency sources with the same intensity. ‘‘Figure. 4’’ shows TPSF time profiles of detectors for three sources. The TPSF’s detected in the left (Detector 5, 6, 7) presents homology form to the other on the right (Detector 3, 2, 1), because the homogeneity in geometrical form (half circle) and optical parameters between form in the left and right, except that the intensity detected in detector 1 is higher than the one in detector 7 which is homologue with the detector 1, even idea for the detector 2 and detector 3 which are homologues to detector 6 and detector 5 respectively, this difference in intensity between each homologues detectors is due to the difference of optical properties between the inclusions of left (μ_a=0.022 [m^{-1}], $\mu_s^{'}$= 2.75 [m^{-1}]) and right (μ_a=0.022 [m^{-1}], $\mu_s^{'}$= 0.55 [m^{-1}]), this two inclusions present tumour in our object. The inclusion in the left is more hampering for signal propagation than the other in the right because the diffusion reduced coefficient ($\mu_s^{'}$) of left inclusion is greater than the other on the right which justifies the intensity decrease between detectors 1, 2, 3 in right and detectors 7, 6, 5 on the left respectively. Indeed, ‘‘Figure. 5’’ shows the variation of mean time of TPSF detected as a function of detection angle of the three sources, In this three curves we observe that the mean time increases when the frequency source decrease. This is due to the increase of width time (WT) of sources (‘‘Figure. 2’’, temporal profile), for source1 WT_1=0.65*10^{-9} [s], source2 WT_2=1.4*10^{-9} [s], and source3 WT_3= 21*10^{-9} [s], thus the width time impulse influences the mean time of TPSF.

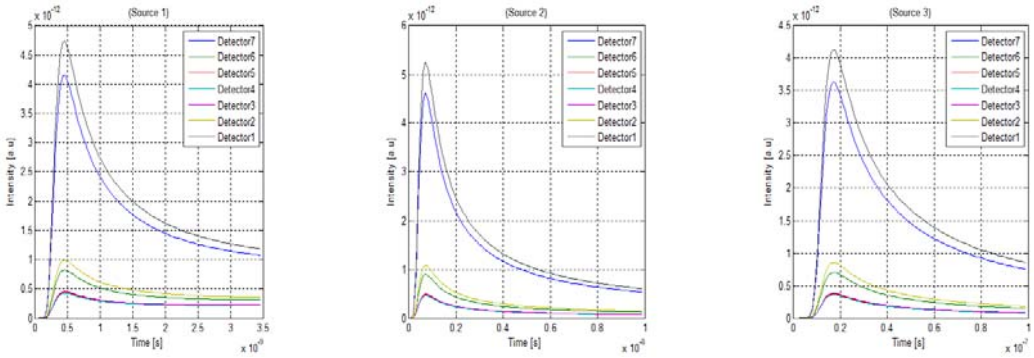

Fig. 4, TPSF time profile of Detectors for three sources.

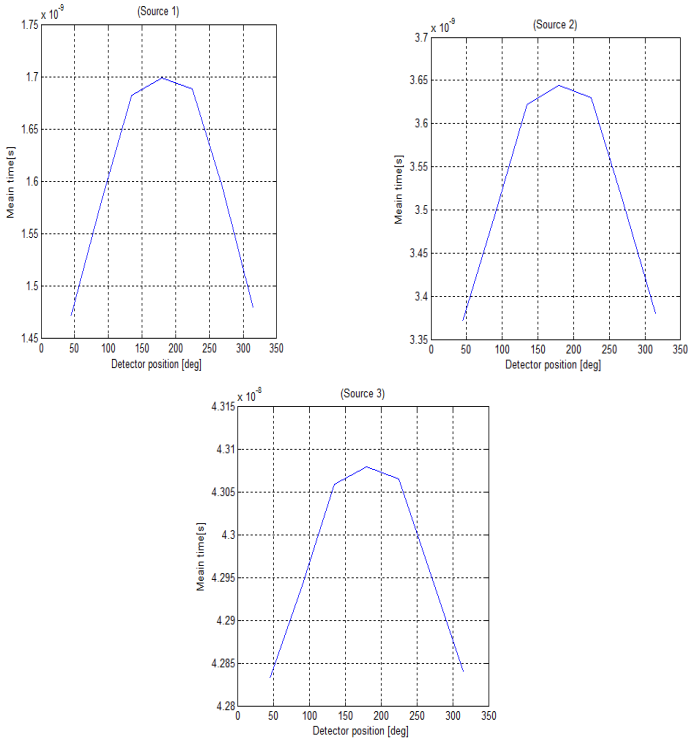

Fig. 5, mean time of TPSF detected with the variation of detection angle for three sources.

Finally, ‘‘Figure. 6’’ shows the mean value and the variance of detected TPSF as a function of detection angle for three sources. We observe that when the source frequency decreases, the mean value and variance of TPSF also decrease and these phenomena are demonstrated physically by the decrease of the source energy.

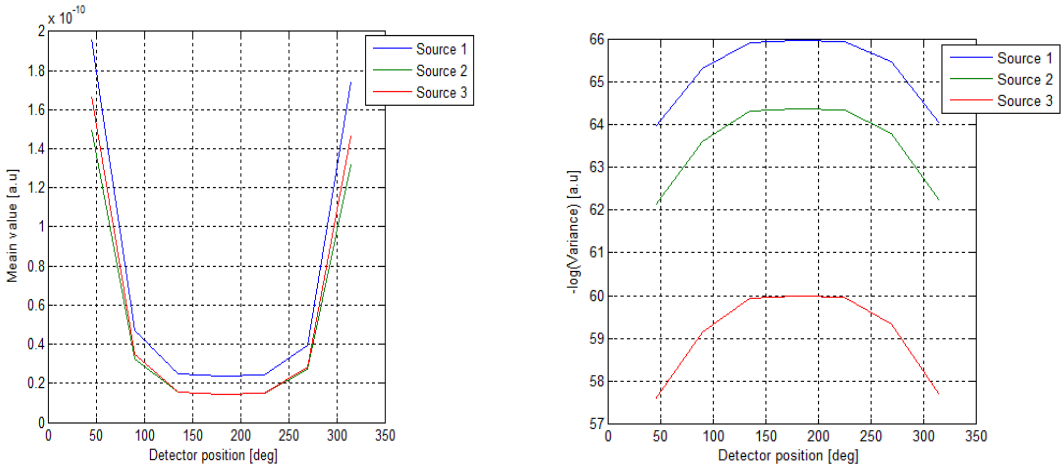

Fig. 6. Variation of mean value and variance of TPSF as a function of detection angle for three sources.

4. Conclusions

The temporal profiles (TPSF) of photons diffused in highly scattering media such as biological tissue, are computed at a base of FEM. This program intended to reconstruct images of the phantoms to be investigated with our time-resolved tomography set up. During the reconstruction process, the parameters of interest, (absorption and reduced diffusion coefficients) will be iteratively adjusted to perform constrained nonlinear minimization of an objective function of the distance between measured and computed temporal profiles. Applications are expected to concern the contribution of resonance magnetic imaging (RMI) in (DOT). Medical applications in cerebral activation are also considered.

References

[1] Herbert Egger And Matthias Schlottbom, Siam J. Math. Anal, **42**, 1934 (2010).
[2] Alexander D. Klose, Journal of Quantitative Spectroscopy & Radiative Transfer **111**, 1852 (2010).
[3]V. Ntziachristos and R. Weissleder, Opt. Lett., **26**, 893 (2001).
[4] X. Montet, J. L. Figueiredo, H. Alencar, V. Ntziachristos and all, Radiology, **242**, 751–758, (2007).
[5] M. A. O'Leary, D. A. Boas, X. D. Li, B. Chance, and A. Yodh, Opt. Lett., **21**, 158 (1996).
[6] R. Roy, A. Godavarty, and E. M. Sevick-Muraca, Phys. Med. Biol., **52**, 4155 (2007).
[7] B. B. Das, F. Liu, and R. R. Alfano, Rep. Prog. Phys., **60**, 227 (1997).
[8] V. Y. Soloviev, J. McGinty, K. B. Tahir, and all, Opt. Lett., **32**, 2034 (2007).
[9] Anand T. N. Kumar, Scott B. Raymond, Andrew K. Dunn, Brian J. Bacskai, David A. Boas, IEEE TRANSACTIONS ON MEDICAL IMAGING, **27**, 1152 (2008).
[10] S.R. Arridge, M. Schweiger, Medical Physics, **20,** 299 (1992).
[11] S.R. Arridge, M. Cope, D.T. Delpy , Physics in medicine and biology, **37**, 1531 (1992).
[12] C. Anastasis, Polycarpou, (book) Printed in the United States of America, **01**, (2006).
[13] M. Schweiger, S.R. Arridge, M. Hiraoka, D.T Deply, Am. Assoc. Phys. Med, **22,** 1779 (1995).
[14] A. Saouli, K. Mansour, IEEE conference proceeding (MMS) 11th, 117– 121, (2011).
[15] B. Joan, C. André, Journal of Quantitative Spectroscopy & Radiative Transfer, **91**, 189 (2005).
[16] Qianqian Fang, Stefan A. Carp, Juliette Selb, and all, IEEE Transactions On Medical Imaging, **28**, 30 (2009).